Coulomb effects in disordered solids

M. F. Thorpe and S. W. de Leeuw*
Department of Physics and Astronomy, Michigan State University, East Lansing, Michigan 48824-1116
(Received 22 November 1985)

We develop a general theory to calculate the vibrational response functions for disordered solids (such as *glasses* and *disordered crystalline alloys)* in the presence of long-range *Coulomb forces.* The longitudinal $\epsilon_l(\omega)$ and transverse $\epsilon_t(\omega)$ dielectric functions are shown to be related by $\epsilon_l(\omega)/\epsilon_\infty = 2-\epsilon_\infty/\epsilon_t(\omega)$, where ϵ_∞ is the high-frequency electronic response. The Lyddane-Sachs-Teller relation is generalized for use in such systems. We derive sum rules involving moments that should be useful in interpreting experimental data. A general formulation is also set up for the density of states $\rho(\omega^2)$ and the neutron scattering law $S(\mathbf{k},\omega)$. These general results are illustrated by calculating these response functions for a model AX_2 glass that roughly corresponds to vitreous silica. A periodic random network with 1536 ions in each supercell is constructed. The response functions are found using the equation-of-motion method with the Coulomb sums included explicitly using the Ewald method. The (bare) transverse response shows a rather broad optic peak whereas the longitudinal response (which is sensitive to the depolarizing field) has a sharper response at a higher frequency.

I. INTRODUCTION

The effect of Coulomb forces on the phonon dispersion curves of crystalline solids is well known. It is most dramatic around $\mathbf{k}=0$ where, in the absence of retardation effects, it leads to the longitudinal-optic (LO) —transverse-optic (TO) splitting. This has been seen in many crystals with ionic charges, and most clearly in inelastic-neutron-scattering experiments as shown for example in Fig. 1 for GaAs.[1]

The Coulomb force is difficult to handle because its long-range nature is sensitive to the *macroscopic shape* of the sample. These effects are manifest at $k \lesssim 1/L$, where L is a linear dimension of the sample. Throughout this paper we neglect retardation, and hence polariton effects, by setting the velocity of light equal to infinity. Even for $k \gtrsim 1/L$, the Coulomb force requires some special techniques developed for crystals by Ewald.[2] These involve isolating the shape-dependent depolarizing terms that only effect the spectrum at $\mathbf{k}=0$. The remaining terms can be judiciously arranged as rapidly convergent short-ranged sums in both real and reciprocal spaces, by the appropriate choice of a free parameter that is introduced. Such lattice-dynamics calculations in crystals are now quite routine.[3]

The situation is much more complicated in *glasses* and *disordered crystalline alloys.* For nearly 10 years there has been experimental evidence of LO-TO splittings in glasses.[4] The responses are broadened but the evidence seems quite compelling and will be discussed in detail

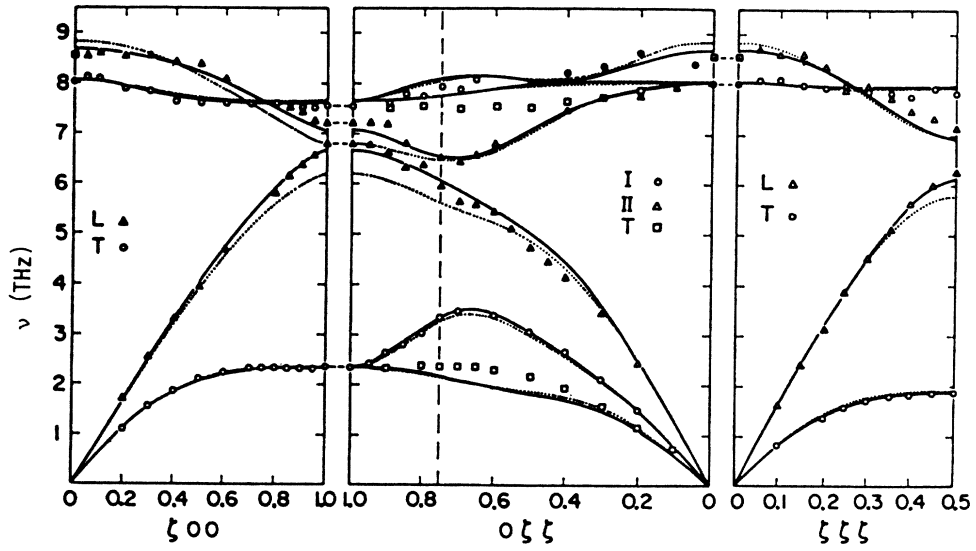

FIG. 1. Phonon dispersion curves for GaAs as measured by inelastic neutron scattering (Ref. 1). The lines are various theoretical fits. The LO-TO splitting is clearly seen in the optic modes. [Reproduced from Bilz and Kress (Ref. 1).] Note 1 THz = 33.4 cm^{-1}.

later. On the other hand, we have found no adequate theoretical treatment despite a number of interesting approaches to the problem.[5,6] The reason for this is clear. The problem is difficult because disordered solids have no *microscopic* translational invariance, so that the Coulomb sums cannot be split up into a part in real space and a part in reciprocal space because the wave vector **k** is no longer a good internal quantum label.

We have tried in this paper to give as comprehensive a treatment as possible. In the next section we express the response functions of interest in terms of the Green functions of the system. Arbitrary displacements are expanded in terms of orthonormal eigenvectors that form a complete set of states but *no use is made of reciprocal space.* Formulas are derived for the various dielectric functions, the density of states, and the inelastic-neutron-scattering cross section.

In Sec. III, the *Coulomb forces* are discussed explicitly. We regard a disordered solid as the limit of a crystal with a large unit cell (supercell) as the size of the supercell goes to infinity. This concept allows the generalized Ewald approach to be easily adapted. It also permits actual numerical computations.

In Sec. IV we discuss *depolarization effects* and show that the longitudinal and transverse dielectric responses are not independent but related. This is useful as the transverse dielectric function can be viewed as the *bare* response of the system in the absence of depolarization effects. We show that this result is consistent with electrostatics

In Sec. V we derive various useful relations between the *moments* of the longitudinal and transverse dielectric response. The main features of the LO-TO splittings and widths can be invoked from these second- and fourth-moment relations. We also generalize the Lydanne-Sachs-Teller (LST) relation to a form that is useful in these systems. We show that the density of states is independent of the sample shape, as would be expected.

In Sec. VI we review the equation-of-motion technique and relate it to the general formulism in Sec. II. Prescriptions are given for the computation of the various response functions of interest.

In Sec. VII we describe the building of a 1536-ion periodic random network with 512 A atoms and 1024 X atoms. This model of an AX_2 glass resembles vitreous silica. The computational difficulties associated with applying the equation-of-motion technique to such a large system with Coulomb forces are discussed.

In Sec. VIII we present the results for the longitudinal and transverse dielectric responses. We use this to verify the various sum rules we have derived. We also show results for the density of states and the neutron-scattering law.

Finally, in the conclusion we make some general comments about the analysis of experimental data in both glasses and disordered crystalline alloys.

II. BASIC FORMULATION

We consider a solid in equilibrium. The fluctuations from some given static structure are described by the Hamiltonian

$$H'=\sum_{i,\alpha}\frac{p_\alpha^2(i)}{2m_i}+\tfrac{1}{2}\sum_{i,j,\alpha,\beta}V_{ij}^{\alpha\beta}u_\alpha(i)u_\beta(j)-\sum_{i,\alpha}q_iu_\alpha(i)E_\alpha\ . \tag{1}$$

The index i labels the ions and subscript α refers to the Cartesian component. The first term is the kinetic energy of the system, where the momentum $p_\alpha(i)$ is the conjugate variable of the displacement $u_\alpha(i)$. The second term is the harmonic part of the potential (including the Coulomb terms) and the last term represents the coupling of an external field **E** to the dipole moment of the system. The polarization **P** of the medium is

$$P_\alpha=\frac{1}{\Omega}\sum_i q_iu_\alpha(i)\ , \tag{2}$$

where the q_i are the ionic charges associated with the point ions and Ω is the volume of the system.[7]

We will now develop standard linear-response theory in a way that is appropriate for disordered systems.[8] The Coulomb forces are "hidden" in the $V_{ij}^{\alpha\beta}$ and will not be considered explicitly until later. The equation of motion from (1) is

$$m_i\ddot{u}_\alpha(i)=-\sum_{\alpha,\beta}V_{ij}^{\alpha\beta}u_\beta(j)+q_iE_\alpha\ . \tag{3}$$

We look for the response at a frequency ω, so setting

$$\begin{aligned}E_\alpha&=E_\alpha^0e^{-i\omega t}\ ,\\ P_\alpha&=P_\alpha^0e^{-i\omega t}\ ,\\ u_\alpha(i)&=u_\alpha^0(i)e^{-i\omega t}\ ,\end{aligned} \tag{4}$$

we can rewrite (3) as

$$\sum_{j,\beta}\frac{V_{ij}^{\alpha\beta}}{(m_im_j)^{1/2}}u_\beta^0(j)-\omega^2u_\alpha^0(i)=\frac{q_i}{(m_i)^{1/2}}E_\alpha^0\ . \tag{5}$$

These linear equations can be solved to yield

$$u_\alpha^0(i)=\sum_{j,\beta}\Gamma_{ij}^{\alpha\beta}\frac{q_jE_\beta^0}{(m_j)^{1/2}}\ , \tag{6}$$

where $\Gamma_{ij}^{\alpha\beta}$ is the inverse of the matrix,

$$\phi_{ij}^{\alpha\beta}=\frac{V_{ij}^{\alpha\beta}}{(m_im_j)^{1/2}}-\omega^2\delta_{\alpha\beta}\delta_{ij}\ , \tag{7}$$

and we identify the first term in Eq. (7) with the usual *dynamical matrix* of the system,

$$D_{ij}^{\alpha\beta}=\frac{V_{ij}^{\alpha\beta}}{(m_im_j)^{1/2}}\ . \tag{8}$$

If we let the eigenvalues of D be λ_n^2 and the corresponding eigenvectors $\xi_n(i,\alpha)$, then

$$\sum_{j,\beta}D_{ij}^{\alpha\beta}\xi_n(j,\beta)=\lambda_n^2\xi_n(i,\alpha)\ , \tag{9}$$

and the $\xi_n(i,\alpha)$ form an orthonormal set,

$$\sum_{i,\alpha}\xi_n^*(i,\alpha)\xi_m(i,\alpha)=\delta_{nm}\ , \tag{10}$$

$$\sum_n \xi_n^*(i,\alpha)\xi_n(j,\beta)=\delta_{\alpha\beta}\delta_{ij} \ . \tag{11}$$

In general, any displacement may be expanded in terms of the eigenvectors, so that we may write

$$u_\alpha^0(i)=\sum_n a_n\xi_n(i,\alpha) \ , \tag{12}$$

where the a_n are the amplitudes of each eigenvector present in the displacement pattern. Inserting (12) into (5) we find that

$$\sum_{j,\beta,n} D_{ij}^{\alpha\beta}a_n\xi_n(j,\beta)-\omega^2\sum_n a_n\xi_n(i,\alpha)=\frac{q_i}{(m_i)^{1/2}}E_\alpha^0 \ ,$$

so that

$$\sum_n a_n(\lambda_n^2-\omega^2)\xi_n(i,\alpha)=\frac{q_iE_\alpha^0}{(m_i)^{1/2}} \ ,$$

and hence

$$a_n=\sum_{j,\beta}\frac{q_jE_\beta^0}{(m_j)^{1/2}}\frac{\xi_n(j,\beta)}{\lambda_n^2-\omega^2} \ . \tag{13}$$

Inserting (13) in (12) and comparing with Eq. (6), we see that

$$\Gamma_{ij}^{\alpha\beta}=\sum_n\frac{\xi_n(i,\alpha)\xi_n^*(j,\beta)}{\lambda_n^2-\omega^2} \ , \tag{14}$$

which accomplishes the appropriate matrix inversion and allows the susceptibility $\chi_{\alpha\beta}$ defined by

$$P_\alpha=\sum_\beta\chi_{\alpha\beta}E_\beta$$

to be written[9]

$$\chi_{\alpha\beta}=\frac{1}{\Omega}\sum_{i,j,n}\frac{q_iq_j}{(m_im_j)^{1/2}}\frac{\xi_n(i,\alpha)\xi_n^*(j,\beta)}{\lambda_n^2-\omega^2} \ . \tag{15}$$

From here the dielectric response is defined by

$$\epsilon=\epsilon_\infty+4\pi\chi \ , \tag{16}$$

which is interpreted as a matrix equation. The quantity ϵ_∞ is the *high-frequency dielectric response* due to the electronic degrees of freedom. It enters both here and in the screening between the charges in the Coulomb terms buried in the potential (1). This will be discussed in more detail in the next section.

It is convenient to reexpress the result (15) in terms of Green functions. Dropping the field term from the Hamiltonian (1) (it was only included in order to develop linear-response theory), the system is described by the Hamiltonian

$$H=\sum_{i,\alpha}\frac{p_\alpha^2(i)}{2m_i}+\tfrac{1}{2}\sum_{i,j,\alpha,\beta}V_{ij}^{\alpha\beta}u_\alpha(i)u_\beta(j) \ . \tag{17}$$

Let $G_{\alpha\beta}(i,j;\omega)$ denote the usual thermal Green function,[9]

$$G_{\alpha\beta}(i,j;\omega)=\langle\langle u_\alpha(i);u_\beta(j)\rangle\rangle_\omega \ , \tag{18}$$

which has the equation of motion

$$m_i\omega^2G_{\alpha\beta}(i,j;\omega)=\delta_{ij}\delta_{\alpha\beta}+\sum_{i',\alpha'}V_{ii'}^{\alpha\alpha'}G_{\alpha'\beta}(i',j;\omega) \ . \tag{19}$$

It is convenient to absorb the masses by setting

$$\tilde{G}_{\alpha\beta}(i,j;\omega)=\left[\frac{m_i}{m_j}\right]^{1/2}G_{\alpha\beta}(i,j;\omega) \ , \tag{20}$$

so that (19) becomes

$$\omega^2\tilde{G}_{\alpha\beta}(i,j;\omega)=\frac{\delta_{ij}\delta_{\alpha\beta}}{m_i}+\sum_{i',\alpha'}\frac{V_{ii'}^{\alpha\alpha'}}{(m_im_i')^{1/2}}\tilde{G}_{\alpha'\beta}(i',j;\omega) \ . \tag{21}$$

Using the results of this section, it is easy to show that

$$\tilde{G}_{\alpha\beta}(i,j;\omega)=\frac{1}{m_i}\sum_n\frac{\xi_n(i,\alpha)\xi_n^*(j,\beta)}{\omega^2-\lambda_n^2} \ , \tag{22}$$

by substituting $\tilde{G}_{\alpha\beta}(i,j;\omega)$ back into Eq. (21). Hence,

$$G_{\alpha\beta}(i,j;\omega)=\frac{1}{(m_im_j)^{1/2}}\sum_n\frac{\xi_n(i,\alpha)\xi_n^*(j,\beta)}{\omega^2-\lambda_n^2} \ , \tag{23}$$

and so Eq. (15) can be rewritten as

$$\chi_{\alpha\beta}=-\frac{1}{\Omega}\sum_{i,j}q_iq_jG_{\alpha\beta}(i,j;\omega) \ , \tag{24}$$

which is the result we want.

Note that the formalism above makes no *assumptions about periodicity* and thus applies to disordered as well as crystalline solids. Examples of disordered, partially ionic, solids are vitreous SiO_2 and the crystalline alloy $Ga_xAl_{1-x}As$. The only assumption made is that the equilibrium position of the ions are well defined so that the harmonic approximation can be made.[10]

Other quantities of interest can also be expressed in terms of the Green functions. The density of states per degree of freedom is defined as

$$\rho(\omega)=2\omega\rho(\omega^2)=\frac{2\omega}{3N}\sum_n\delta(\omega^2-\lambda_n^2)$$
$$=-\frac{2\omega}{3\pi N}\mathrm{Im}\left[\sum_{n,i,\alpha}\frac{\xi_n(i,\alpha)\xi_n^*(i,\alpha)}{\omega^2-\lambda_n^2}\right] . \tag{25}$$

Therefore,

$$\rho(\omega)=-\frac{2\omega}{3\pi N}\sum_{i,\alpha}m_i\mathrm{Im}G_{\alpha\alpha}(i,i;\omega) \ . \tag{26}$$

It is also useful to define parallel and perpendicular **k**-dependent susceptibilities by generalizing the result (24) so that

$$\chi^{\parallel}(\mathbf{k},\omega)=-\frac{1}{\Omega}\sum_{i,j,\alpha,\beta}q_iq_j\hat{k}_\alpha^{\parallel}\hat{k}_\beta^{\parallel}G_{\alpha\beta}(i,j;\omega)e^{i\mathbf{k}\cdot\mathbf{R}_{ij}} \ , \tag{27}$$

$$\chi^{\perp}(\mathbf{k},\omega)=-\frac{1}{\Omega}\sum_{i,j,\alpha,\beta}q_iq_j\hat{k}_\alpha^{\perp}\hat{k}_\beta^{\perp}G_{\alpha\beta}(i,j;\omega)e^{i\mathbf{k}\cdot\mathbf{R}_{ij}} \ , \tag{28}$$

where $\hat{k}_\alpha^{\parallel}$ is the αth component of a unit vector *parallel* to the wave vector **k**, and $\hat{k}_\alpha^{\perp}$ is the αth component of a unit vector *perpendicular* to **k**. The vector R_i describes the equilibrium position of the site i and $R_{ij}=R_i-R_j$. The **k**-dependent longitudinal and transverse dielectric responses then become

$$\epsilon_l(\mathbf{k},\omega)=\epsilon_\infty(\mathbf{k})+4\pi\chi^{\parallel}(\mathbf{k},\omega)\ . \tag{29}$$

We write

$$\epsilon_t(\mathbf{k},\omega)=\epsilon_\infty(\mathbf{k})+4\pi\chi^{\perp}(\mathbf{k},\omega)\ , \tag{30}$$

where $\epsilon_\infty(\mathbf{k})$ is the low-frequency limit of the electronic response of the system.

Finally, we can express the neutron-scattering law[11] $S(\mathbf{k},\omega)$ in terms of the Green function. The *coherent* cross section is[11,12]

$$S^{\rm coh}(\mathbf{k},\omega)=-\frac{1}{\pi}\mathrm{Im}\left[\sum_{i,j,\alpha,\beta}\hat{k}_\alpha\hat{k}_\beta a_i^{\rm coh}a_j^{\rm coh}\times G_{\alpha\beta}(i,j;\omega)e^{i\mathbf{k}\cdot\mathbf{R}_{ij}}\right], \tag{31}$$

where $a_i^{\rm coh}$ is the coherent scattering length of the ion at site i. The *incoherent* cross section is given by

$$S^{\rm inc}(\mathbf{k},\omega)=-\frac{1}{\pi}\mathrm{Im}\left[\sum_{i,\alpha}(\hat{k}_\alpha)^2(a_i^{\rm inc})^2G_{\alpha\alpha}(i,i;\omega)\right], \tag{32}$$

where $a_i^{\rm inc}$ is the incoherent scattering length.

A number of reasonable simplifications have been made in the theory developed in this section that we will now discuss. We assume that we can make the Born-Oppenheimer[13] approximation and treat the electronic and vibrational degree of freedom separately. Because the electronic excitations have much larger energy than the phonons, we are at *low frequencies for the electrons,* even when well above the phonon absorption band. Therefore it is reasonable to take ϵ_∞, the electronic contribution to the dielectric function, to be the *low-frequency limit* of the electronic dielectric function. This treatment is applicable to insulators and semiconductors.

In order to make progress possible, we have also suppressed the $\mathbf{k}$ dependence in ϵ_∞. This is reasonable for wavelengths larger than the atomic size. Major changes would have to be made in the current work to include the $\mathbf{k}$ dependence of ϵ_∞. This may be necessary in the future when more detailed comparisons are made between theory and experiment at shorter wavelengths. The distinctive effects of Coulomb forces are manifest at very small $\mathbf{k}\to\mathbf{0}$, so that in this limit the $\mathbf{k}$ dependence of ϵ_∞ can be safely ignored.

Another k-dependent effect is the Debye-Waller factor.[11,13] Higher-order processes lead to a term

$$\exp[-\tfrac{1}{2}k^2\langle u_\alpha^2(i)\rangle_\omega] \tag{33}$$

being associated with the α degree of freedom of the ion at i, where $\langle\ \rangle_\omega$ indicates the contribution to the thermal average at a frequency ω. These factors should be incorporated into Eqs. (27)—(32). They *cannot* be included within the equation-of-motion method, although they can be handled within more conventional molecular dynamics where the complete, rather than the one-phonon response is calculated. Again for small k, the Debye-Waller factors can all be set equal to 1, which we do in this paper.

Finally, we comment on the role of temperature. Because we are working within the *harmonic approximation,* the temperature enters in a simple way. The density of states and the various susceptibilities and dielectric functions are *temperature independent.* The neutron-scattering cross sections (30) and (31) contain Bose factors $n(\omega)$ or $n(\omega)+1$ (where $n(\omega)=[\exp(\beta\hbar\omega)-1]^{-1}$) for phonon destruction or creation. These thermal prefactors have been suppressed. Thus we make the conceptual simplification of working at zero temperature in this paper. This simplifies the algebra and emphasizes that we are working with essentially classical systems.

III. THE ELECTROSTATIC ENERGY

In this section we derive expressions for the electrostatic energy of a supercell with periodic boundary conditions. We consider a cubic supercell with volume $\Omega=L^3$ containing N ions of charge q_i $(i=1,2,\ldots,N)$ with instantaneous positions $\mathbf{r}_i$. Electrical neutrality is assumed. The electrostatic energy of the cell under periodic boundary conditions is then given by

$$V_c=\frac{1}{2\epsilon_\infty}\sum_{\mathbf{n}}\sum_{i=1}^{N}\sum_{j=1}^{N}{}'\frac{q_iq_j}{|\mathbf{r}_{ij}+\mathbf{n}|}\ . \tag{34}$$

The sum is over all translation vectors $\mathbf{n}=(n_1,n_2,n_3)$ L of the simple-cubic superlattice and all ions i and j inside the cell. The prime on the summation symbol $\sum'$ indicates that the term $i=j$ is to be excluded in the sum when $\mathbf{n}=\mathbf{0}$, and ϵ_∞ represents the screening by the electrons in the ions, which is assumed to occur instantaneously.

As pointed out by de Leeuw *et al.*,[14] the right-hand side of Eq. (34) forms a conditionally convergent series and is thus meaningless without further specification. In particular, we need to specify the order of the various terms in Eq. (34). This can be done by introducing an appropriate convergence factor. For example, de Leeuw *et al.* employed a spherical convergence factor e^{-sn^2} in evaluating Eq. (34). They showed that the result in that case corresponds to the electrostatic energy of a cubic cell at the center of an array of replicas[15] arranged such that all replicas form a macroscopically large sphere. Alternatively,

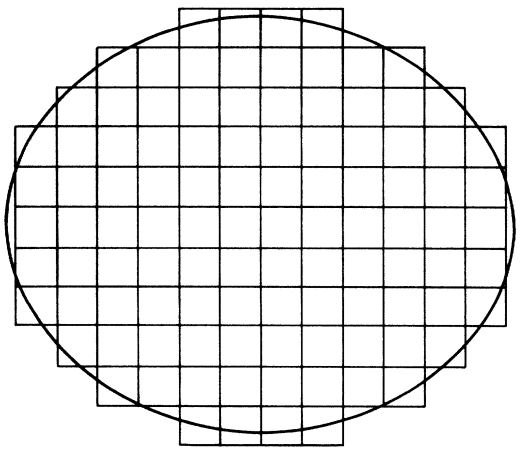

FIG. 2. Ellipsoidal macroscopic sample is covered by supercells whose centers fall *inside* the ellipsoid.

we can consider a large but finite number of replicas and sum over a specified set of translation vectors $\mathbf{n}$ (e.g., all translation vectors for which $|\mathbf{n}| \leq K$). Questions of convergence then do not arise as one only considers a finite sum. One then tries to find an asymptotic series in descending powers of K retaining the leading terms only. In both techniques the shape of the system enters in a natural way. This is to be expected since shape effects do enter into the solution of electrostatic problems. It is precisely because of this that we can uniquely relate the response of our system in an external field to the dielectric function.[16]

For our purpose it is convenient to generalize the results of de Leeuw *et al.*[14] and Smith[15] to systems having an *ellipsoidal shape.* Each supercell is periodically repeated within the macroscopic ellipsoid as shown schematically in Fig. 2. The technique of convergence factors is mathematically somewhat simpler, so that we use this method. Accordingly, we introduce an ellipsoidal convergence factor and seek a rapidly convergent expression for

$$V_c(s)=\frac{1}{2\epsilon_\infty}\sum_{\mathbf{n}}\sum_{i=1}^{N}\sum_{j=1}^{N}{}' \frac{q_i q_j}{|\mathbf{r}_{ij}+\mathbf{n}|}\exp\left[-s\left[\frac{n_1^2}{a^2}+\frac{n_2^2}{b^2}+\frac{n_3^2}{c^2}\right]L^2\right] \tag{35}$$

in the limit $s\to 0$. We use the identity

$$\frac{1}{|\mathbf{r}|}=\frac{1}{\sqrt{\pi}}\int_0^\infty dt\, t^{-1/2}e^{-r^2 t} \tag{36}$$

and Jacobi's transformation for Θ functions:[17]

$$\sum_{l=-\infty}^{\infty} e^{-(x+l)^2 t}=(\pi/t)^{1/2}\sum_{l=-\infty}^{\infty} e^{-\pi^2 l^2/t+2\pi i l x}\,. \tag{37}$$

The manipulations are exactly the same as described by de Leeuw *et al.*[14] and will not be repeated here. The result is

$$V_c(s)=V_c^{\mathrm{I}}(s)+V_c^{\mathrm{II}}(s)+V_c^{\mathrm{III}}(s)\,, \tag{38}$$

$$V_c^{\mathrm{I}}(0)=\frac{1}{2\epsilon_\infty}\sum_{\mathbf{n}}\sum_{i=1}^{N}\sum_{j=1}^{N}{}' \frac{q_i q_j}{|\mathbf{r}_{ij}+\mathbf{n}|}\operatorname{erfc}(\eta|\mathbf{r}_{ij}+\mathbf{n}|)-\frac{\eta}{\epsilon_\infty\sqrt{\pi}}\sum_i q_i^2\,, \tag{39a}$$

$$V_c^{\mathrm{II}}(0)=\frac{1}{\pi\Omega\epsilon_\infty}\sum_{\mathbf{k}\neq 0}\frac{\exp(-\pi^2|\mathbf{k}|^2/\eta^2)}{|\mathbf{k}|^2}\left|\sum_{j=1}^{N} q_j\exp(2\pi i\mathbf{k}\cdot\mathbf{r}_j)\right|^2\,, \tag{39b}$$

$$V_c^{\mathrm{III}}(s)=\frac{\pi abc}{2\Omega\epsilon_\infty}\sum_{i=1}^{N}\sum_{j=1}^{N} q_i q_j\int_0^\infty\frac{dt}{\sqrt{t}}\frac{\exp\{-st[x_{ij}^2/(a^2t+s)+y_{ij}^2/(b^2t+s)+z_{ij}^2/(c^2t+s)]\}}{[(a^2t+s)(b^2t+s)(c^2t+s)]^{1/2}}\,. \tag{39c}$$

In Eqs. (39a) and (39b) we have set $s=0$. Here, $\operatorname{erfc}(x)$ denotes the complementary error function

$$\operatorname{erfc}(x)=(2/\sqrt{\pi})\int_x^\infty dx\, e^{-x^2}\,.$$

The sum $\sum_{\mathbf{k}\neq 0}$ is over all reciprocal-lattice vectors of the simple-cubic lattice $\mathbf{k}=(k_1,k_2,k_3)/L$ excluding $\mathbf{k}=0$. The disposable parameter η governs the rate of convergence of the series. Its numerical value is chosen to optimize convergence. To obtain an asymptotic expression for $V_c^{\mathrm{III}}(s)$ we expand the exponential function in the integrand in powers of st. The first term $[O(s^{-1})]$ vanishes because of charge neutrality. The second term can be written as

$$-\frac{\pi abc}{\Omega\epsilon_\infty}\sum_{i=1}^{N}\sum_{j=1}^{N} q_i q_j(B_x x_{ij}^2+B_y y_{ij}^2+B_z z_{ij}^2)\,, \tag{40a}$$

with

$$B_x=\tfrac{1}{2}abcs\int_0^{\eta^2} dt\frac{\sqrt{t}}{(a^2t+s)^{3/2}(b^2t+s)^{1/2}(c^2t+s)^{1/2}}\,, \tag{40b}$$

and similar expressions for B_y and B_z. The integral can be transformed by the substitution $t=s/v$. Letting $s\to 0$, we then obtain

$$B_x=\tfrac{1}{2}abc\int_0^\infty\frac{dv}{(a^2+v)^{3/2}(b^2+v)^{1/2}(c^2+v)^{1/2}}\,, \tag{41}$$

which is the usual depolarization factor[16,18] along the x axis for an ellipsoid with semiaxes a,b,c. Equivalent results are obtained for B_y and B_z. All higher-order terms are easily shown to vanish as $s\to 0$. Using the charge-neutrality condition, we have that

$$-\sum_{i=1}^{N}\sum_{j=1}^{N} q_i q_j x_{ij}^2=2\left[\sum_{i=1}^{N} q_i x_i\right]^2\,,$$

which gives

$$V_c^{\mathrm{III}}(0)=\frac{2\pi}{\Omega\epsilon_\infty}\left[B_x\left[\sum_{i=1}^{N} q_i x_i\right]^2+B_y\left[\sum_{i=1}^{N} q_i y_i\right]^2+B_z\left[\sum_{i=1}^{N} q_i z_i\right]^2\right]\,. \tag{42}$$

This is the generalization of the results of de Leeuw *et al.*[14] and Smith[15] to ellipsoidal geometry. For the case $a=b=c$ (spherical geometry), it is easily shown that $B_x=B_y=B_z=\frac{1}{3}$, whereas in slab geometry ($a,b\to\infty$), we

have $B_x=B_y=0$ and $B_z=1$. As expected, our result for the electrostatic energy is identical to the result obtained by Ewald apart from the term V_c^{III} containing the depolarization factors.

The dipolar contribution to the harmonic Hamiltonian equation (17) can now be obtained by differentiating twice with respect to the displacements $\mathbf{u}_i$ of the ions from their equilibrium positions $\mathbf{R}_i$. The result is

$$
\begin{aligned}
V_{dd}=&\frac{1}{4\epsilon_\infty}\sum_{\mathbf{n}}\sum_{i=1}^{N}{\sum_{j=1}^{N}}' q_iq_j(u_i-u_j)^2F(|\mathbf{R}_i-\mathbf{R}_j+\mathbf{n}|)\\
&-\frac{1}{4\epsilon_\infty}\sum_{\mathbf{n}}\sum_{i=1}^{N}{\sum_{j=1}^{N}}' q_iq_j[(u_i-u_j)\cdot(\mathbf{R}_i-\mathbf{R}_j+\mathbf{n})]^2H(\mathbf{R}_i-\mathbf{R}_j+\mathbf{n})\\
&+\frac{2\pi}{\Omega\epsilon_\infty}\sum_{\mathbf{k}\neq 0}\frac{\exp(-\pi^2|\mathbf{k}|^2/\eta^2)}{|\mathbf{k}|^2}\left|\sum_{j=1}^{N}q_j(\mathbf{u}_j\cdot\mathbf{k})e^{2\pi i\mathbf{k}\cdot\mathbf{R}_j}\right|^2\\
&-\frac{2\pi}{\Omega\epsilon_\infty}\sum_{\mathbf{k}\neq 0}\frac{\exp(-\pi^2|\mathbf{k}|^2/\eta^2)}{|\mathbf{k}|}\left[\sum_{j=1}^{N}q_j(\mathbf{k}\cdot\mathbf{u}_j)^2e^{-2\pi i\mathbf{k}\cdot\mathbf{R}_j}\right]\left[\sum_{j=1}^{N}q_je^{2\pi i\mathbf{k}\cdot\mathbf{R}_j}\right]\\
&+\frac{2\pi}{\Omega\epsilon_\infty}\left[B_x\left[\sum_{i=1}^{N}q_iu_{ix}\right]^2+B_y\left[\sum_{i=1}^{N}q_iu_{iy}\right]^2+B_z\left[\sum_{i=1}^{N}q_iu_{iz}\right]^2\right], \qquad (43)
\end{aligned}
$$

where

$$F(x)=\frac{1}{x^3}\left[\frac{2\eta x}{\sqrt{\pi}}e^{-\eta^2x^2}+\mathrm{erfc}(\eta x)\right]$$

and

$$H(x)=\frac{1}{x^5}\left[\frac{2\eta x}{\sqrt{\pi}}(2\eta^2x^2+3)e^{-\eta^2x^2}+3\,\mathrm{erfc}(\eta x)\right].$$

We have used Eqs. (38) and (39) for the minimization of the energy of our networks, whereas Eq. (43) was used in the computation of the response functions with the equation-of-motion technique. The practical implementation of these lattice sums in computer simulations has been discussed elsewhere.[19] Here we note the Ewald sum, and particularly the part in reciprocal space, is eminently suited for *vector processing.*

IV. DEPOLARIZATION EFFECTS

In this section we show that the dielectric response of the system, with the shape-dependent terms *included,* can be expressed in terms of the dielectric response function with the shape-dependent terms *excluded.* A special case of this theorem expresses the *longitudinal dielectric response* in terms of the *transverse dielectric response.* This is useful in saving computational time and leads to useful insights. The theorem is proved by using the *separability*[20] of the shape-dependent terms in the potential. The result is shown to be consistent with known electrostatic results.

From the work of the preceding section, we see that the Hamiltonian [Eq. (17)] can be written as

$$H=H_0+U\ , \qquad (44)$$

where H_0 is the part of the Hamiltonian that is *independent* of the *shape* of the macroscopic sample and U is the shape-dependent part which may be written

$$U=\frac{2\pi}{\Omega\epsilon_\infty}\sum_{\alpha=1}^{3}B_\alpha\left[\sum_i q_iu_\alpha(i)\right]^2, \qquad (45)$$

where, from Eq. (41), the depolarizing factors B_α obey the sum rule

$$\sum_{\alpha=1}^{3}B_\alpha=1\ . \qquad (46)$$

The potential (45) is *separable* which allows the shape dependence to be included in the dielectric function in *closed form.*

We form the dynamical matrix D_0 from H_0 [see Eq. (8)] and hence define P by

$$\underline{P}^{-1}=\underline{M}\omega^2-\underline{D}_0\ . \qquad (47)$$

We also define the Green function for the complete Hamiltonian (44) via

$$\underline{G}^{-1}=\underline{M}\omega^2-\underline{D}_0-\underline{U}\ , \qquad (48)$$

where the matrix elements of $\underline{U}$ are the second derivatives formed from Eq. (45). Thus we have, from (47) and (48),

$$\underline{G}=\underline{P}+\underline{P}\,\underline{U}\,\underline{G}\ . \qquad (49)$$

Consider for the moment only the B_x term in Eq. (45), and then in components,

$$
\begin{aligned}
G_{xx}(i,j;\omega)=&P_{xx}(i,j;\omega)\\
&+\sum_{j',j''}P_{xx}(i,j';\omega)\frac{4\pi}{\Omega\epsilon_\infty}B_xq_{j'}q_{j''}G_{xx}(j'',j;\omega)\ . \qquad (50)
\end{aligned}
$$

We multiply this equation by q_iq_j and sum over i,j. The separability of the potential means that we can solve to obtain

$$\sum_{i,j}q_iq_jG_{xx}(i,j;\omega)=\frac{\sum_{i,j}q_iq_jP_{xx}(i,j;\omega)}{1-(4\pi B_x/\Omega\epsilon_\infty)\sum_{i,j}q_iq_jP_{xx}(i,j;\omega)}\ . \qquad (51)$$

This remarkable result relates the dielectric response of the system *with* and *without* the depolarizing terms. In

calculating the response in the x direction, we have used only the B_x terms. The B_y and B_z terms do not influence the x response in systems with *high macroscopic symmetry*. Examples of such systems are vitreous silica, which is macroscopically *isotropic* and the crystalline alloy $Ga_xAl_{1-x}As$, which is macroscopically *cubic*. However, lower-symmetry systems can be easily handled by going to principal axes, in which the x, y, and z components decouple.

Using Eqs. (16) and (24), the result (51) can be written

$$\epsilon_x(\omega)-\epsilon_\infty=\frac{\epsilon(\omega)-\epsilon_\infty}{1+(B_x/\epsilon_\infty)[\epsilon(\omega)-\epsilon_\infty]} . \tag{52}$$

It is useful to regard the usual dielectric response $\epsilon(\omega)$ as the *bare response*. The response $\epsilon_x(\omega)$ includes the effects of the macroscopic depolarization field through B_x.

From Eq. (46), we have the useful sum rule

$$\frac{\epsilon(\omega)+2\epsilon_\infty}{\epsilon(\omega)-\epsilon_\infty}=\sum_{\alpha=1}^{3}\frac{\epsilon_\infty}{\epsilon_\alpha(\omega)-\epsilon_\infty} . \tag{53}$$

For the special case of a sphere, this sum rule reduces to the Clausius-Mossotti[13,18] form

$$\frac{\epsilon(\omega)-\epsilon_\infty}{\epsilon(\omega)+2\epsilon_\infty}=\frac{1}{3}\left[\frac{\epsilon_x(\omega)-\epsilon_\infty}{\epsilon_\infty}\right] , \tag{54}$$

where $\epsilon_x(\omega)=\epsilon_y(\omega)=\epsilon_z(\omega)$ is the response including depolarizing effects.

An especially important case is that of slab geometry, where $B_x=B_y=0$ and $B_z=1$. The transverse response is the bare response $\epsilon(\omega)$ from Eq. (52),

$$\epsilon_t(\omega)=\epsilon(\omega) . \tag{55}$$

The longitudinal response $\epsilon_l(\omega)$ is given, from Eq. (52), by

$$\frac{\epsilon_l(\omega)}{\epsilon_\infty}=2-\frac{\epsilon_\infty}{\epsilon(\omega)} . \tag{56}$$

These are probably the most important results in this paper. It means that the usual dielectric function $\epsilon(\omega)$ can be calculated as the *transverse* dielectric function of a slab with *no* depolarizing effects and then the longitudinal response can be found directly from Eq. (56). Although only the bare response need be calculated, this is by no means easy. Even though the shape-dependent terms have been eliminated, the short-ranged parts of the Coulomb forces in real and reciprocal space still have to be included.

The result (52) and hence those that follow, (53)–(56), are consistent with electrostatics, which can be seen as follows. If an external field E_0 is applied to a sample with a depolarizing factor B_x in the x direction, then the electric field inside $E_{\rm in}$ is reduced and given by

$$E_0=\epsilon_\infty E_{\rm in}+4\pi B_x P . \tag{57}$$

This comes from the continuity of the electric displacement D. The polarization P is defined by

$$P=\frac{\epsilon-\epsilon_\infty}{4\pi}E_{\rm in} . \tag{58}$$

However, in our computations the polarization is defined in terms of the *external* applied field E_0,

$$P=\frac{\epsilon_x-\epsilon_\infty}{4\pi\epsilon_\infty}E_0 . \tag{59}$$

From (57)–(59), we see that

$$\frac{\epsilon_\infty}{\epsilon_x-\epsilon_\infty}=\frac{\epsilon_\infty}{\epsilon-\epsilon_\infty}+B_x ,$$

which is the zero-frequency limit of the result (52). This is not surprising since we assumed the speed of light to be infinite; electrostatics becomes valid at *all* frequencies.

V. MOMENT SUM RULES

In this section we prove a number of sum rules involving moments and we also find a generalization of the Lyddane-Sachs-Teller[21] (LST) relation that is suitable for use in disordered systems which have a continuum rather than a discrete dielectric response. We start with Eq. (44), where the system is described by $H=H_0+U$, where U is the depolarizing term (45) and

$$H_0=\sum_{i,\alpha}\frac{P_\alpha^2(i)}{2mi}+\tfrac{1}{2}\sum_{i,j,\alpha,\beta}V_{ij}^{\alpha\beta}u_\alpha(i)u_\beta(j) \tag{60}$$

is everything else [see Eq. (17)].

From the results of Sec. II, it is clear that

$$\frac{1}{\pi}\int_0^\infty {\rm Im}\epsilon_x(\omega)d\omega^2=\frac{4\pi}{\Omega}\sum_{i,j,n}\frac{q_iq_j}{(m_im_j)^{1/2}}\xi_n(ix)\xi_n^*(jx)$$
$$=\frac{4\pi}{\Omega}\sum_i\frac{q_i^2}{m_i}=\omega_p^2 \tag{61}$$

is independent of the depolarizing term B_x and therefore the same for all directions. As we are most interested in the transverse response $\epsilon_t(\omega)$ and the longitudinal response $\epsilon_l(\omega)$, we have

$$\frac{1}{\pi}\int_0^\infty {\rm Im}\epsilon_t(\omega)d\omega^2=\frac{1}{\pi}\int_0^\infty {\rm Im}\epsilon_l(\omega)d\omega^2=\omega_p^2 , \tag{62}$$

where the *bare* plasma frequency ω_p^2 is defined in (61).

The second moment can be found similarly,

$$\frac{1}{\pi}\int_0^\infty \omega^2{\rm Im}\epsilon_x(\omega)d\omega^2=\frac{4\pi}{\Omega}\sum_{i,j,n}\frac{q_iq_j}{(m_im_j)^{1/2}}\xi_n(i,x)\lambda_n^2\xi_n^*(j,x)=\frac{4\pi}{\Omega}\sum_{\substack{i,j,n\\ j',\alpha}}\frac{q_iq_j}{(m_im_j)^{1/2}}\xi_n(j',\alpha)\left[V_{ij'}^{x\alpha}+\frac{4\pi B_x}{\Omega\epsilon_\infty}q_iq_j\delta_{\alpha x}\right]\xi_n^*(j,x)$$
$$=\frac{4\pi}{\Omega}\sum_{i,j}\frac{q_iq_j}{m_im_j}V_{ij}^{xx}+\left[\frac{4\pi}{\Omega}\right]^2\frac{B_x}{\epsilon_\infty}\sum_{i,j}\frac{q_i^2q_j^2}{m_im_j}=\frac{1}{\pi}\int_0^\infty\omega^2{\rm Im}\epsilon_t(\omega)d\omega^2+\frac{B_x}{\epsilon_\infty}\omega_p^4 . \tag{63}$$

Defining the moments of $\mathrm{Im}\epsilon_x(\omega)$ in the usual way,

$$\langle\omega^n\rangle_x=\frac{(1/\pi)\int_0^\infty \omega^n \mathrm{Im}\epsilon_x(\omega)d\omega^2}{(1/\pi)\int_0^\infty \mathrm{Im}\epsilon_x(\omega)d\omega^2}\ , \tag{64}$$

we can immediately see that

$$\langle\omega^2\rangle_x-\langle\omega^2\rangle=B_x\omega_p^2/\epsilon_\infty\ , \tag{65}$$

where $\langle\omega^2\rangle_t=\langle\omega^2\rangle$ is the second moment of the bare response with $B_x=0$. Setting $B_x=1$, we find the expected result,

$$\langle\omega^2\rangle_l-\langle\omega^2\rangle_t=\omega_p^2/\epsilon_\infty\ , \tag{66}$$

which is a generalization of the result in a simple, partially ionic crystal like GaAs where the transverse and longitudinal responses consist of single δ functions. Note that the bare plasma frequency is screened by ϵ_∞ in (66).

The fourth moment can be evaluated in a similar way. After some tedious algebra and using the result (65), we find that

$$\langle\omega^4\rangle_x-\langle\omega^2\rangle_x^2=\langle\omega^4\rangle-\langle\omega^2\rangle^2\ , \tag{67}$$

where $\langle\omega^4\rangle_t=\langle\omega^4\rangle$ is the bare response. This result shows that the variance is *independent* of the depolarizing term B_x. A special case of (67) is

$$\langle\omega^4\rangle_l-\langle\omega^2\rangle_l^2=\langle\omega^4\rangle_t-\langle\omega^2\rangle_t^2\ . \tag{68}$$

The real part of the dielectric constant can be obtained from the imaginary part via the Kramers-Kronig[9] relation,

$$\epsilon'(\omega)=\mathrm{Re}\epsilon(\omega)=\epsilon_\infty+\frac{1}{\pi}\int_0^\infty \frac{\mathrm{Im}\epsilon_t(\omega')}{(\omega')^2-\omega^2}d(\omega')^2\ . \tag{69}$$

Thus the zero-frequency dielectric constant ϵ_0 is given by

$$\epsilon_0=\epsilon_\infty+\omega_p^2\left\langle\frac{1}{\omega^2}\right\rangle_t\ . \tag{70}$$

Similarly, for the longitudinal response we have a similar relation,

$$\epsilon_0^l=\epsilon_\infty+\omega_p^2\left\langle\frac{1}{\omega^2}\right\rangle_l\ , \tag{71}$$

where ϵ_0^l is the zero-frequency limit of the longitudinal dielectric constant. However, from the zero-frequency limit of (69), we have

$$\frac{\epsilon_0^l}{\epsilon_\infty}=2-\frac{\epsilon_\infty}{\epsilon_0}\ , \tag{72}$$

so that from Eqs. (77)—(79) we derive the important result

$$\frac{\epsilon_0}{\epsilon_\infty}=\frac{\langle 1/\omega^2\rangle_t}{\langle 1/\omega^2\rangle_l}\ , \tag{73}$$

which generalizes the LST result for a simple crystal like GaAs to a disordered solid with a continuous spectrum. We note that the LST form for an ionic crystal with a large unit cell,[22]

$$\frac{\epsilon_0}{\epsilon_\infty}=\prod_i\frac{\omega_{li}^2}{\omega_{ti}^2}\ , \tag{74}$$

is very *different* from (73) when the number of terms in the product is greater than one. We have found no useful way to generalize (74). It is a quite unusual relationship because it only involves the positions of the peaks and *not* their weights.

The higher moments of $\mathrm{Im}\epsilon_x(\omega)$ for $n>4$ can also be found by the method at the beginning of this section. However, it becomes increasingly difficult for large n. For the longitudinal and transverse responses it can be done more easily using the result (55). From the Kramers-Kronig relation (69), it is easy to see by expanding the energy denominator in the integrand that

$$\frac{\epsilon_t(\omega)}{\epsilon_\infty}=1-\frac{\omega_p^2}{\epsilon_\infty\omega^2}\sum_{r=0}^\infty\frac{\langle\omega^{2r}\rangle_t}{\omega^{2r}}\ , \tag{75}$$

and similarly for the longitudinal response,

$$\frac{\epsilon_l(\omega)}{\epsilon_\infty}=1-\frac{\omega_p^2}{\epsilon_\infty\omega^2}\sum_{r=0}^\infty\frac{\langle\omega^{2r}\rangle_l}{\omega^{2r}}\ . \tag{76}$$

These high-frequency series converge at frequencies down to the top of the phonon band when the dielectric response becomes complex.

The relation (56) can be written

$$\left[2-\frac{\epsilon_l(\omega)}{\epsilon_\infty}\right]\frac{\epsilon_t(\omega)}{\epsilon_\infty}=1\ . \tag{77}$$

Inserting the series (75) and (76) into (77) and reorganizing slightly leads to the moment-generating equation,

$$\sum_{r=0}^\infty\left[\frac{\langle\omega^{2r}\rangle_l-\langle\omega^{2r}\rangle_t}{\omega^{2r}}\right]=\frac{\omega_p^2}{\epsilon_\infty\omega^2}\left[\sum_{r=0}^\infty\sum_{s=0}^\infty\frac{\langle\omega^{2r}\rangle_l\langle\omega^{2s}\rangle_t}{\omega^{2r+2s}}\right]\ . \tag{78}$$

Equation powers of ω, we find the moment relation

$$\langle\omega^{2r}\rangle_l-\langle\omega^{2r}\rangle_t=\frac{\omega_p^2}{\epsilon_\infty}\sum_{p=0}^{r-1}\langle\omega^{2r-2-2p}\rangle_l\langle\omega^{2p}\rangle_t\ . \tag{79}$$

The first few of these are

$$r=1:\ \langle\omega^2\rangle_l-\langle\omega^2\rangle_t=\omega_p^2/\epsilon_\infty\ , \tag{80}$$

$$r=2:\ \langle\omega^4\rangle_l-\langle\omega^4\rangle_t=\omega_p^2/\epsilon_\infty(\langle\omega^2\rangle_l+\langle\omega^2\rangle_t)\ , \tag{81}$$

$$r=3:\ \langle\omega^6\rangle_l-\langle\omega^6\rangle_t=\omega_p^2/\epsilon_\infty(\langle\omega^4\rangle_l+\langle\omega^2\rangle_l\langle\omega^2\rangle_t+\langle\omega^4\rangle_t)\ . \tag{82}$$

We note that (80) is the same as (66) found earlier in this section, while (81) and (82) together can be rewritten to yield (68).

Finally, we comment on the density of states $\rho(\omega)$ defined via, say, Eq. (25). In a crystalline solid, $\rho(\omega)$ is independent of the depolarizing terms B_α because only a vanishingly small part of the spectrum with $k\lesssim 1/L$ is affected by finite-size effects, where L is a linear dimension of the sample. Thus as $L\to\infty$ the density of states becomes shape independent. We would intuitively expect this to be true in a disordered solid also. It is most easily proved by noting that all the moments $\langle\omega^{2r}\rangle$ of $\rho(\omega^2)$ defined by

$$\langle\omega^{2r}\rangle=\int_0^\infty \rho(\omega^2)\omega^{2r}d\omega^2 \tag{83}$$

are *independent* of the B_α. Using (25), we can write

$$\langle\omega^{2r}\rangle=\sum_{n,i,\alpha}\xi_n(i,\alpha)\lambda_n^{2r}\xi_n^*(i,\alpha)\ . \tag{84}$$

Thus,

$$\langle\omega^{2r}\rangle=\mathrm{Tr}(\underline{D}_0+\underline{U})^r\ , \tag{85}$$

where the trace is over sites i and Cartesian components α, and

$$(\underline{D}_0+\underline{U})_{ij}^{\alpha\beta}=\frac{V_{ij}^{\alpha\beta}}{(m_im_j)^{1/2}}+\frac{4\pi B_\alpha}{\epsilon_\infty\Omega}\frac{q_iq_j}{(m_im_j)^{1/2}}\delta_{\alpha\beta}\ . \tag{86}$$

Thus $\langle\omega^2\rangle$ is independent of the B_α because of charge neutrality, and the higher moments contain the B_α terms with the volume factor Ω and, so in the limit of large volume we have the expected results that the density of states is *shape independent.*

The B_α terms enter the moment expressions for the density of states and the dielectric function in different ways because the dielectric function involves sum over off-diagonal terms in the Green function and has extra weighting factors q_i and q_j. Thus we have the result that the density of states is independent of the B_α, whereas the dielectric function is not.

VI. EQUATION-OF-MOTION TECHNIQUE

The equation-of-motion technique[23,24] is a variant of conventional molecular dynamics that is useful in disordered harmonic systems like those under consideration here. Unlike molecular dynamics, the system does not have to be left for some time to come into equilibrium before the response is monitored. Instead, the initial conditions at $t=0$ are determined by the particular response function it is desired to calculate, and the equations are integrated forward in time with appropriate weighting factors. The method is by now well known and we summarize its use in the present context. This treatment and notation follows Beeman and Alben.[24]

The harmonic equations of motion for the Hamiltonian (17) are

$$m_i\ddot{u}_{i\alpha}(t)=-\sum_{j,\beta}V_{ij}^{\alpha\beta}u_{j\beta}(t)\ , \tag{87}$$

where $u_{i\alpha}$ is the displacement of the ith atom in the α direction. Note that the $u_{i\alpha}$ in this section is equivalent to the $u_\alpha(i)$ used previously. It is convenient to think of the $u_{i\alpha}$ as *classical* displacements. The result is the same for classical and quantum systems, except for the thermal factors, as was discussed in Sec. II. These thermal factors occur in a simple way in a harmonic systems as prefactors and can be included later. The motion in this system can be written as a superposition of normal-mode vibrations. Thus,

$$u_{i\alpha}(t)=[1/(m_i)^{1/2}]\sum_n q_n\xi_n(i,\alpha)\cos(\omega_nt+\delta_n)\ . \tag{88}$$

Here, ω_n is the frequency of the nth normal mode and δ_n the phase shift; q_n is the amplitude of the nth normal mode and $\xi_n(i,\alpha)$ is the magnitude of the nth eigenvector on particle i in the α direction. The dynamical matrix is real and symmetric, so that its eigenvectors can be chosen to be *real.* They are orthonormal and obey Eqs. (10) and (11).

Let the initial positions at $t=0$ be denoted by $u_{i\alpha}^0$. The initial velocities are set equal to zero. It follows immediately that all phase factors vanish. Hence $\delta_0=0$ for all n. Therefore,

$$u_{i\alpha}(t)=[1/(m_i)^{1/2}]\sum_n q_n\xi_n(i,\alpha)\cos(\omega_nt)\ , \tag{89}$$

$$u_{i\alpha}^0=[1/(m_i)^{1/2}]\sum_n q_n\xi_n(i,\alpha)\ , \tag{90}$$

which can be inverted with the closure relations (10) and (11):

$$q_n=\sum_{i,\beta}m_j^{1/2}u_{j\beta}^0\xi_n(i,\alpha)\ . \tag{91}$$

Now compute

$$G(\omega)=\frac{2}{\pi}\int_0^T dt\cos(\omega t)e^{-\lambda(t/T)^2}\sum_{i,\alpha}A_{i\alpha}u_{i\alpha}(t)\ , \tag{92}$$

where the amplitudes $A_{i\alpha}$ will be chosen later to yield the appropriate response function. Using (89) and (90), we obtain

$$\sum_{i,\alpha}A_{i\alpha}u_{i\alpha}(t)=\sum_{i,\alpha}\sum_{j,\beta}\sum_n\left[\frac{m_j}{m_i}\right]^{1/2}\xi_n(i,\alpha)\times\xi_n(j,\beta)A_{i\alpha}u_{j\beta}^0\cos(\omega_nt)\ . \tag{93}$$

Then,

$$G(\omega)=\sum_{i,\alpha}\sum_{j,\beta}\sum_n\left[\frac{m_j}{m_i}\right]^{1/2}\xi_n(i,\alpha)\xi_n(j,\beta)\times A_{i\alpha}u_{j\beta}^0[\Delta(\omega-\omega_n)+\Delta(\omega+\omega_n)]\ , \tag{94}$$

and

$$\Delta(\omega)=\frac{1}{\pi}\int_0^T\cos(\omega t)e^{-\lambda(t/T)^2}dt\ . \tag{95}$$

Clearly,

$$\lim_{\lambda\to0^+}\lim_{T\to\infty}\Delta(\omega)\to\delta(\omega)\ . \tag{96}$$

For finite T and λ, $\Delta(\omega)$ is sharply peaked at $\omega=0$ with small oscillations or ripples at other frequencies. Depending on our choice of $A_{i\alpha}$ and $u_{i\alpha}^0$, $G(\omega)$ represents a weighted sum over the density of states and we can thus compute various quantities of interest. A list of these is given below.

A. Density of states

Let $u_{i\alpha}^0=A_{i\alpha}=\sqrt{2}\cos\theta_{i\alpha}$, where $\theta_{i\alpha}$ is a random angle uniformly distributed in the interval $0\le\theta_{i\alpha}\le2\pi$. Averaging over many sets of random angles leads to

$$\langle\cos\theta_{i\alpha}\cos\theta_{j\beta}\rangle_{\mathrm{av}}=\tfrac{1}{2}\delta_{ij}\delta_{\alpha\beta}\ . \tag{97}$$

Hence,

$$\langle G(\omega)\rangle_{\rm av}=\sum_n\sum_{i,\alpha}\xi_n^2(i,\alpha)[\Delta(\omega-\omega_n)+\Delta(\omega-\omega_n)]$$
$$=\sum_n[\Delta(\omega-\omega_n)+\Delta(\omega+\omega_n)]\ , \tag{98}$$

which is the density of states $\rho(\omega)$ defined by Eq. (26). In practice, large systems are self-averaging and it is unnecessary to average over different sets of random numbers.

B. Dielectric constant

Let

$$u_{i\alpha}^0=\hat{E}_\alpha q_i/m_i\ , \tag{99}$$

$$A_{i\alpha}=\hat{E}_\alpha q_i \tag{100}$$

Then,

$$G(\omega)=\sum_n\left|\sum_{i,\alpha}\frac{q_i\xi_n(i\alpha)\hat{E}_\alpha}{(m_i)^{1/2}}\right|^2[\Delta(\omega+\omega_n)+\Delta(\omega-\omega_n)]\ . \tag{101}$$

Here, $\hat{\mathbf{E}}$ is a unit vector in the direction of the electric field of the incident light. If we use slab geometry,

$$\mathrm{Im}[\epsilon(\omega)-1]=\frac{2\pi^2}{\Omega\omega}G(\omega),\ \hat{\mathbf{E}}\text{ parallel to slab} \tag{102}$$

$$\mathrm{Im}[1-\epsilon^{-1}(\omega)]=\frac{2\pi^2}{\Omega\omega}G(\omega),\ \hat{\mathbf{E}}\text{ perpendicular to slab}\ . \tag{103}$$

The real parts of Eqs. (102) and (103) can be obtained from the imaginary part through Kramers-Kronig transformation:

$$\mathrm{Re}f(\omega_0)=\frac{2}{\pi}\int_0^\infty\frac{\omega f''(\omega)-\omega_0 f''(\omega_0)}{\omega^2-\omega_0^2}d\omega\ , \tag{104}$$

where $f''(\omega)$ is the imaginary part of $f(\omega)$ which stands for either $\epsilon(\omega)-1$ or $1-\epsilon^{-1}(\omega)$. This form of the Kramers-Kronig transform conveniently avoids problems when $\omega=\omega_0$.

C. Dynamic structure factor $S(\mathbf{k},\omega)$

Let

$$u_{i\alpha}^0=\frac{\hat{k}_\alpha}{m_i}e^{i\mathbf{k}\cdot\mathbf{r}_i}\ , \tag{105}$$

$$A_{i\alpha}=\hat{k}_\alpha e^{-i\mathbf{k}\cdot\mathbf{r}_i}\ . \tag{106}$$

Then

$$G(\omega)=\sum_n\left|\sum_{i,\alpha}\frac{\hat{k}_\alpha\xi_n(i\alpha)e^{i\mathbf{k}\cdot\mathbf{r}_i}}{(m_i)^{1/2}}\right|^2$$
$$\times[\Delta(\omega-\omega_n)+\Delta(\omega+\omega_n)]\ , \tag{107}$$

which is the dynamic structure factor $S(\mathbf{k},\omega)$, with the thermal Bose factors and Debye-Waller factors suppressed as discussed earlier. The coherent- and incoherent-neutron-scattering laws can be found in a similar way by incorporating the appropriate scattering lengths.

D. Longitudinal dielectric function $\epsilon_l(\mathbf{k},\omega)$

Setting

$$u_{i\alpha}^0=\frac{q_i\hat{k}_\alpha}{m_i}e^{i\mathbf{k}\cdot\mathbf{r}_i}\ , \tag{108}$$

$$A_{i\alpha}=q_i\hat{k}_\alpha e^{-i\mathbf{k}\cdot\mathbf{r}_i}\ , \tag{109}$$

$$G(\omega)=\sum_n\left|\sum_{i,\alpha}\frac{q_i\hat{k}_\alpha\xi_n(i\alpha)e^{-i\mathbf{k}\cdot\mathbf{r}_i}}{(m_i)^{1/2}}\right|^2$$
$$\times[\Delta(\omega+\omega_n)+\Delta(\omega-\omega_n)]\ . \tag{110}$$

The longitudinal dielectric function is

$$\mathrm{Im}\epsilon_l(\mathbf{k},\omega)=\frac{2\pi^2}{\Omega\omega}G(\omega)\ . \tag{111}$$

The real part can be obtained through a Kramers-Kronig transformation like (104).

E. Transverse dielectric function $\epsilon_t(\mathbf{k},\omega)$

We write

$$u_{i\alpha}^0=\frac{q_i\hat{k}_\alpha^\perp}{m_i}e^{i\mathbf{k}\cdot\mathbf{r}_i}\ , \tag{112}$$

$$A_{i\alpha}=q_i\hat{k}_\alpha^\perp e^{-i\mathbf{k}\cdot\mathbf{r}_i}\ , \tag{113}$$

where $\hat{\mathbf{k}}^\perp$ is a unit vector perpendicular to $\mathbf{k}$. Then,

$$G(\omega)=\sum_n\left|\sum_{i,\alpha}\frac{q_i\hat{k}_\alpha^\perp\xi_n(i,\alpha)}{(m_i)^{1/2}}e^{i\mathbf{k}\cdot\mathbf{r}_i}\right|^2$$
$$\times[\Delta(\omega-\omega_n)+\Delta(\omega+\omega_n)]\ , \tag{114}$$

$$\mathrm{Im}\epsilon_t(\mathbf{k},\omega)=\frac{2\pi^2}{\Omega\omega}G(\omega)\ , \tag{115}$$

and the real part can be obtained through the Kramers-Kronig transformation like (104).

VII. CONSTRUCTION OF PERIODIC RANDOM NETWORKS

In this section we describe the construction of a random network with periodic boundary conditions. Consider a cubic cell containing a sufficiently large number (N) of atoms (in our case, 216 or 512) on a cubic diamond lattice.

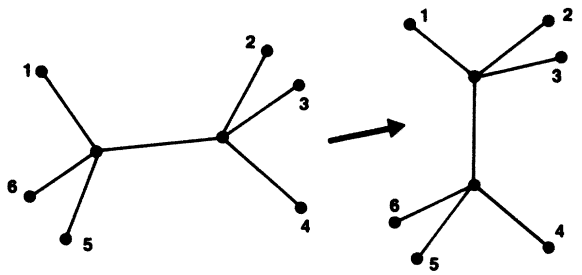

FIG. 3. Construction proposed by Wooten and Weaire (Ref. 25) for building random networks in which the bonds from the two unlabeled atoms in the center of the labeled exterior atoms are reorganized as shown. Four six-membered rings are changed into two pairs of five- and seven-membered rings.

Each atom is fourfold coordinated and the structure contains six-membered rings only. Periodic boundary conditions apply. It is possible to alter the topology of the network and still retain fourfold coordination for all atoms. This is done by introducing topological defects[25–27] of the kind shown in Fig. 3. Here we sketch how the local topology can be changed by simply reconnecting two bonds. It is easily checked that in this process four six-membered rings are altered into two five- and two seven-membered rings. Repeated introduction of these defects leads eventually to a structure which is no longer recognizable as a crystalline solid. Eventually, the ring statistics settle to values which are not unreasonable. For a fuller description we refer to the work of Wooten and Weaire,[25] who first proposed this construction, and He.[26,27]

The advantages of this construction are clear:

(i) Fourfold coordination is maintained throughout the construction of the network and no dangling bonds are introduced.

(ii) Periodic boundary conditions can be maintained throughout to obtain a random network with periodic boundary conditions.

(iii) The local strain caused by the introduction of a defect is expected to be small after relaxation.

The spontaneous formation of such defects has been observed recently in a molecular-dynamics simulation on Ge by Stillinger and Weber.[28]

Periodic boundary conditions do impose some restrictions on the network. One would expect these restrictions to become less important as the number of atoms in the supercell increases. We did observe a long-lived memory of the original diamond lattice. We found some memory of the original diamond lattice to persist indefinitely when the network was not large enough. This could be seen most clearly by monitoring the structure factors $S(\mathbf{k})$,

$$S(k)=\frac{1}{N}\sum_{j=1}^{N}\sum_{l=1}^{N}\exp[i\mathbf{k}\cdot(\mathbf{r}_j-\mathbf{r}_l)]\ , \tag{116}$$

as more and more defects are introduced. Because of the periodic boundary conditions, $S(\mathbf{k})$ can be computed only at supercell positions $\mathbf{k}=(2\pi/L)(n_1,n_2,n_3)$, where the n_i are integers. Initially, $S(\mathbf{k})$ vanishes unless the Bragg condition for the original diamond lattice is met. As more topological defects are introduced, some intensity is observed at other points in reciprocal space and the intensity in the Bragg reflections diminishes. For an amorphous network there should be no Bragg reflections. Thus the intensity at points in $\mathbf{k}$ space corresponding to Bragg reflections of the original diamond lattice should not be radically different from other points in reciprocal space. We used this as our criterion to judge whether the supercell had lost memory of the original diamond lattice. It was impossible to meet this condition if the network did not contain a sufficiently large number of atoms. Only for networks containing 512 atoms or more could all Bragg reflections be reduced in intensity to the general level. To accomplish this it was necessary to introduce a large number of defects (~ 10 defects per atom). Note that defects can be made on top of defects.

A SiO_2-like network was created by placing anions along the bonds between the fourfold-coordinated atoms. The resulting supercell contained 1024 twofold-coordinated anions and 512 fourfold-coordinated cations. The network was relaxed with a potential of the form

$$V=\frac{3}{8}\frac{\alpha}{d^2}\sum_{\langle l,\Delta\rangle}(\mathbf{r}_l^2(\Delta)-d^2)+\frac{3}{8}\sum_{\langle l,\Delta,\Delta'\rangle}\frac{\beta_l}{d^2}(\mathbf{r}_{l\Delta}\cdot\mathbf{r}_{l\Delta'}-d^2\cos\theta_l)^2+\sum_{\langle l,m\rangle}A_{lm}\exp(-|\mathbf{r}_{lm}|/\rho)+\frac{1}{\epsilon_\infty}\sum_{\langle l,m\rangle}\frac{q_lq_m}{|\mathbf{r}_{lm}|}\ . \tag{117}$$

The first two terms in Eq. (117) describe changes in energy due to bond stretching (α) and angular forces (β). They have a form suggested by Keating.[29] Here, $\mathbf{r}_l(\Delta)$ denotes a vector from an ion l to near neighbor Δ; d is the equilibrium bond length and θ_l the equilibrium bond angle. The third term describes the short-range repulsion due to the overlap of the electron clouds of ions l and m; A_{lm} reflects the strength of the repulsion and the steepness parameter ρ its range. A repulsive potential is necessary to maintain the stability of the network when Coulomb forces are included. The last term describes the Coulomb interaction between ions l and m with charge q_l and q_m, respectively. The interaction is screened by the high-frequency dielectric charge ϵ_∞. The angular brackets $\langle\ \rangle$ denote that each pair or triplet is only computed once. Values of the parameters in the potential are given in Table I. They were chosen to correspond roughly to v-

TABLE I. Parameters in the potential, Eq. (116).

$\alpha=8.5\times10^4$ dyn/cm	$A_{++}-A_{--}=0$
$\beta_+=\beta_-=3\times10^4$ dyn/cm	$A_{+-}=1.0174\times10^{-9}$ erg
$d=1.65$ Å	$\rho=0.3$ Å
$\theta_+=109.5°$	$q_+=-2q_-=3.67e$
$\theta_-=155°$	$\epsilon_\infty=2.10$

TABLE II. Details of the relaxed network discussed in Sec. VII.

Number of cations:	512
Number of anions:	1024
Box length:	28.5 Å
Molar volume:	27.2 cm^3
Mean nearest-neighbor distance:	1.65±0.04 Å
Mean angle at four-coordinated ion:	109.5°±9.8°
Mean angle at two-coordinated ion:	151.0°±12.5°
Mass of anion:	16 amu
Mass of cation:	28 amu

SiO_2. For later reference we mention that this potential gives a LO-TO splitting of 160 cm^{-1} for the highest split pair in α-quartz, which is close to the experimentally observed value[30] of 163 cm^{-1}. To reproduce the lattice dynamics of α-quartz a model more sophisticated than (117) is required.[31] Our main goal was an investigation of the LO-TO splittings in vitreous materials. The agreement with the observed splitting of the LO-TO pair in α-quartz was deemed sufficient for our purpose.

The network was relaxed with the method of steepest descents.[32] This method is equivalent to finding the long-time solution to the equation of motion:

$$\dot{\mathbf{r}}_i = -\nabla_i V . \tag{118}$$

The Coulomb energy and forces were computed from the results of Sec. III, the expression for the forces being obtained by straightforward differentiation of Eq. (38). The salient features of the network obtained are given in Table II. The molar volume at which the potential energy V is minimal (27.2 cm^3/mole) was made to agree closely with the experimentally observed value of 27.3 cm^3/mole for v-SiO_2. The mean nearest-neighbor distance $\bar{l}=1.65$ is somewhat larger than experimentally[33] observed $\bar{l}=1.61$, and the spread $\Delta l=0.04$ Å. The deviation $\Delta\theta=9.8°$ for the silicon angle is much larger than experimentally observed. This appears to be an endemic problem with networks generated by "amorphising" crystals.[26,27] More work needs to be done to understand this more completely. The mean value and spread of the angle at the oxygen ions is reasonable.

VIII. DYNAMIC RESPONSE OF THE NETWORK

We now discuss the dynamic properties of the network described in the preceding section. Various response functions, such as the density of states, the dielectric function, and the dynamic structure factor, were computed numerically using the equation-of-motion technique. The results serve to illustrate many of the ideas developed in the preceding section. In addition, we give evidence for the existence of well-differentiated long-wavelength transverse- and longitudinal-optic modes in disordered networks. Finally, we present numerical evidence confirming the analysis of the preceding section.

The potential (117) was expanded to second order in the displacements $u_\alpha(i)$ of the ions from their equilibrium positions. For the computation of the dipolar interactions of the displacement dipoles, we used Eq. (43) with a depolarizing factor corresponding to slab geometry with the z axis perpendicular to the slab. Thus $B_x=B_y=0$ and $B_z=1$. The equations of motion were integrated numerically with Verlet's algorithm.[34] Time step $\Delta t=5$ fsec was chosen. The evolution of the initial state was followed for $600\Delta t$ in the case of response functions at zero wave vector and $300\Delta t$ otherwise. This leads to a resolution width $\Delta\omega$ of 28 cm or 56 cm^{-1}, respectively, for the relevant spectral functions.

A convenient unit of frequency is the bare plasma frequency ω_p defined by Eq. (61). With the parameters of our model, we find $\omega_p=939$ cm^{-1}. For the resolution width $\Delta\omega$ we find $0.03\omega_p$ and $0.06\omega_p$, respectively.

In Fig. 4 we show the imaginary parts of the transverse and longitudinal dielectric functions $\epsilon_t(\mathbf{k},\omega)$ and $\epsilon_l(\mathbf{k},\omega)$ at finite wavelength. They were computed for wave vectors of the form $\mathbf{k}=2\pi(0,0,\kappa)/L$, with $\kappa=1$, 2, 3, and 5. The imaginary part of the transverse dielectric function $\epsilon_t''(\mathbf{k},\omega)$ has a well-defined peak at $\omega=1.16\omega_p$. The peak position is seen to be almost independent of wave number κ, but its intensity decreases with increasing κ. For $\omega\lesssim\omega_p$, $\epsilon_t''(\mathbf{k},\omega)$ has a broad peak at $\omega=0.74\omega_p$. As the wave number increases, this peak broadens until only a broad band is observed for $\kappa=5$. Note that the region $\omega>1.05\omega_p$ remains well separated from the rest of the spectrum.

The imaginary part of the longitudinal dielectric function $\epsilon_l''(\mathbf{k},\omega)$ displays a strikingly different behavior. A

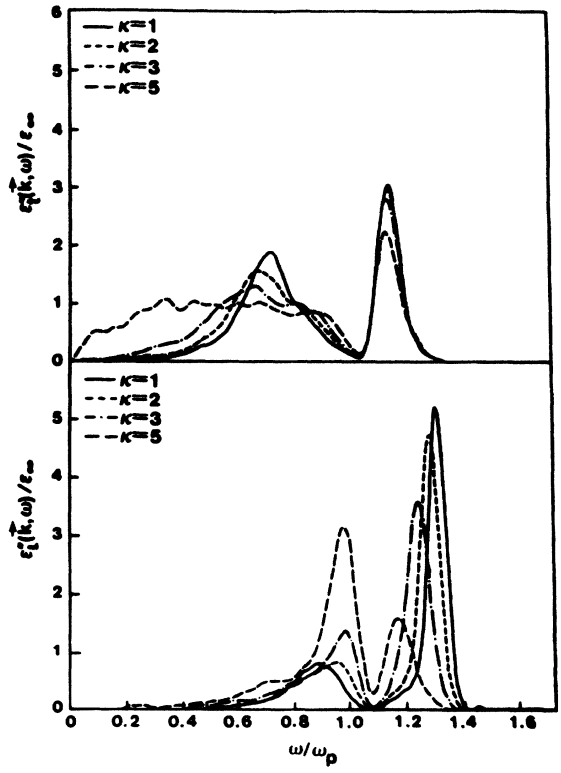

FIG. 4. Imaginary parts of the transverse and longitudinal dielectric functions of wave vectors of the form $\mathbf{k}=2\pi(0,0,\kappa)/L$.

negative dispersion is observed for the high-frequency optic peak similar to that observed in many crystalline materials. This peak is sharp at long wavelengths but broadens and decreases in intensity at shorter wavelengths. The broad peak observed in the region $\omega \lesssim 1.05\omega_p$ at long wavelengths develops into an increasingly well-defined peak at shorter wavelengths, in marked contrast with the behavior of $\epsilon_t''(\mathbf{k},\omega)$.

We have checked that at *finite* wavelength the dielectric functions $\epsilon_l(\mathbf{k},\omega)$ and $\epsilon_t(\mathbf{k},\omega)$ are independent of the magnitude of the depolarizing field in Eq. (43). This was verified by computing $\epsilon_l''(\mathbf{k},\omega)$ and $\epsilon_t''(\mathbf{k},\omega)$ for the longest wave vector accessible in a test network containing only 648 ions with and without the depolarization field. The results came out to be identical within the numerical accuracy of the computation. This independence of boundary conditions was noted earlier by de Leeuw and Perram[35] in their study of charge-density fluctuations of molten salts. It can be made plausible by noting that the depolarization term in Eq. (43) is proportional to the square of the dipole moment per unit volume. For plane-wave-like displacement patterns the total dipole moment will be small, so that this term has little effect on the response functions at finite wavelength. For crystalline materials with a center of symmetry the total dipole moment will be identically zero for these displacement patterns.

Although at finite wavelength our results are independent of the precise form of the depolarization field, this is no longer true in the limit of infinite wavelength. This is illustrated most clearly for the case of slab geometry, for which $B_x = B_y = 0$ and $B_z = 1$ in Eq. (43). Thus the depolarization field acts in the z direction only. We now compute $\epsilon_l''(\mathbf{0},\omega)$ and $\epsilon_t''(\mathbf{0},\omega)$, where l and t refer to the z axis. The depolarization field acts to increase the restoring forces for longitudinal vibrations but has no effect on transverse vibrations. This is illustrated in Fig. 5, where we have plotted $\epsilon_l''(\mathbf{0},\omega)$ and $\epsilon_t''(\mathbf{0},\omega)$. Note that both are smooth extrapolations of the results at finite wavelengths. Only for slab geometry is the extrapolation to $\mathbf{k}=\mathbf{0}$ smooth for both $\epsilon_l(\mathbf{k},\omega)$ and $\epsilon_t(\mathbf{k},\omega)$. The transverse dielectric function $\epsilon_t''(\mathbf{0},\omega)$ has a well-defined peak at $\omega = 1.17\omega_p$, with a full width at half height (FWHH) of $0.09\omega_p$ *after deconvolution,* with the resolution function of width $\Delta\omega = 0.03\omega_p$ introduced by the finite-time truncation in our simulation. A much broader response is observed centered at $\omega = 0.76\omega_p$. The longitudinal dielectric function $\epsilon_l''(0,\omega)$ has a remarkably sharp peak at $\omega = 1.32\omega_p$ with a FWHH of only $0.04\omega_p$ *after deconvolution.* A weak broad response centered at $\omega = 0.88\omega_p$ is seen. These results, combined with the results at finite wavelength, provide unambiguous evidence for the existence of well-differentiated longitudinal- and transverse-optic response with wavelength much longer than the nearest-neighbor separation. The splitting of the highest LO-TO pair is $0.15\omega_p$ (or 140 cm^{-1}), which is only slightly less than the splitting of the highest LO-TO pair in α-quartz. The magnitude of the splitting agrees well with the experimentally observed value.

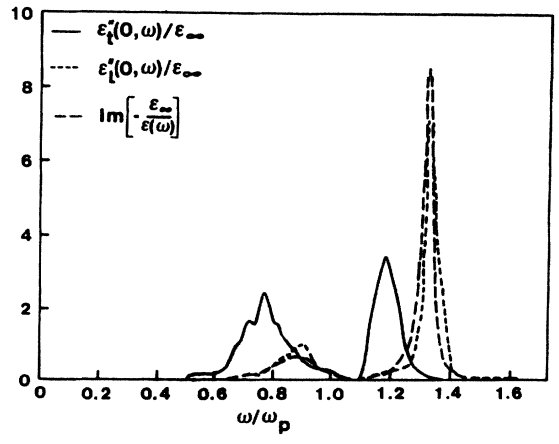

FIG. 5. Long-wavelength limits of imaginary parts of the transverse and longitudinal dielectric functions. Also shown is the imaginary part of the loss function, $\text{Im}[-\epsilon_\infty/\epsilon(\omega)]$.

In the limit of vanishing wave number, $\epsilon_t(\mathbf{k},\omega)$ and $\epsilon_l(\mathbf{k},\omega)$ are not independent. The arguments developed in Sec. IV show that $\epsilon_t(\mathbf{0},\omega)$ can be identified with the bare dielectric response function $\epsilon(\omega)$, whereas Eq. (56) relates $\epsilon_l(\mathbf{0},\omega)$ to $\epsilon(\omega)$. In Fig. 5, a plot of $\text{Im}[-\epsilon_\infty/\epsilon(\omega)]$ is shown which agrees well, within the expanded computational limits, with $\epsilon_l''(\mathbf{0},\omega)/\epsilon_\infty$. This confirms the usefulness of the analysis of Galeener and Lucovsky,[4] who identified the peak in $-\text{Im}\epsilon^{-1}(\omega)$ as longitudinal-optic excitation.

For completeness we show the real part $\epsilon'(\omega)$ of the dielectric function in Fig. 6. A negative region is observed for $1.21\omega_p < \omega < 1.31\omega_p$. In this reststrahlen band, electromagnetic radiation cannot propagate in the glass. We obtain a value $\epsilon_0/\epsilon_\infty = 1.57$ for the static dielectric constant.

In Fig. 7 we show the variation of the peak frequencies ω_{LO} and ω_{TO} for the highest LO-TO pair. The negative dispersion of the LO response is clearly visible, whereas the transverse response shows almost no dispersion. This behavior is reflected in the variation of the second moments $\langle\omega^2(k)\rangle$ of $\epsilon_l''(\mathbf{k},\omega)$ with wave numbers, also shown in Fig. 7. In the long-wavelength limit we recover the sum-rule equation (80):

$$\lim_{\mathbf{k}\to 0}[\langle\omega^2(\mathbf{k})\rangle_l - \langle\omega^2(\mathbf{k})\rangle_t] = \omega_p^2/\epsilon_\infty \ . \tag{119}$$

If the optic responses were δ functions, as in GaAs, then

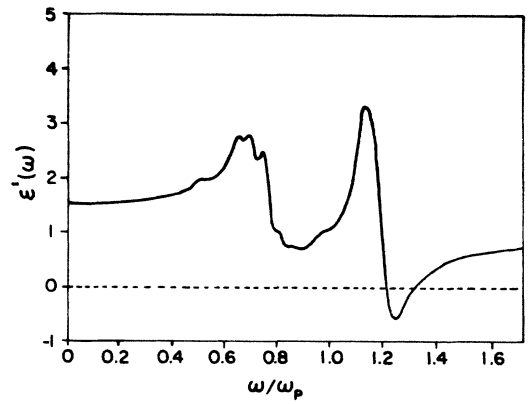

FIG. 6. Real part of the dielectric function $\epsilon'(\omega)$.

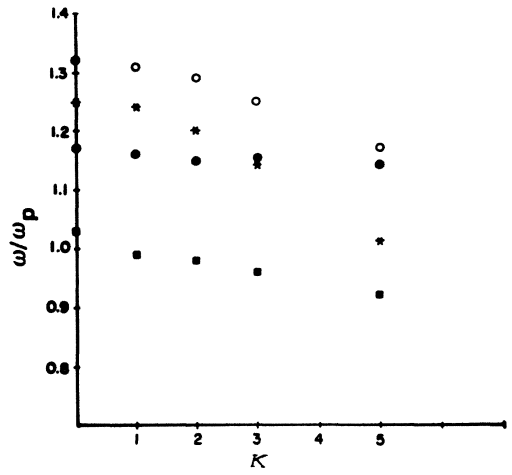

FIG. 7. Variation of the peak frequencies $\bar{\omega}(k)$ and second moments $\langle\omega^2(k)\rangle$ of the imaginary parts of the transverse and longitudinal dielectric response, where open circles denote $\bar{\omega}_{\rm LO}(k)$, solid circles denote $\bar{\omega}_{\rm TO}(k)$, asterisks denote $[\langle\omega^2(k)\rangle_{\rm LO}]^{1/2}$, and solid squares denote $[\langle\omega^2(k)_{\rm TO}]^{1/2}$ and $\mathbf{k}=2\pi(0,0,\kappa)/L$.

the peak frequencies would be given by the second moments. This clearly is *not* the case, as shown by the results in this section and summarized in Fig. 7.

We have also verified that the generalized LST relation, Eq. (73), is obeyed. Specifically, we find a value of 1.61 for the rhs of Eq. (73), which compares well with the experimental ratio $\epsilon_0/\epsilon_\infty=1.57$. The computations lead to a value for the *ratio* $\epsilon_0/\epsilon_\infty$. If we use the value of $\epsilon_\infty=2.10$ as in Table I, we find that $\epsilon_0=3.38$, which is close to be experimental value of 3.30.

The density of states (DOS), $\rho(\omega)$, of the model is shown in Fig. 8. It was computed by averaging over three sets of random initial conditions with the prescription given in Sec. VI A. The DOS is characterized by a broad band $\omega\lesssim 1.05\omega_p$ and a peak at $\omega=1.15\omega_p$, i.e.. close to the TO peak frequency. Thus the transverse-optic modes produce a peak in the density of states. The longitudinal-optic peak, on the other hand, merely serves to define the upper band edge. These observations agree with experiments on v-SiO_2 and v-GeO_2.[4] Experimentally,[36] an additional peak is seen in the weighted density of states in the region between the LO and TO frequencies. This is probably due to optically inactive modes of the kind known to exist in crystalline quartz in this frequency region. Our rigid-ion model places these modes near the TO mode at 1080 $\rm cm^{-1}$ (i.e., $1.15\omega_p$) in α-quartz.[30] The parameters of our model would have to be further refined to move this peak to a higher frequency.

The result for the density of states is seen to be rather noisy in the low-frequency band, but very smooth for $\omega\gtrsim\omega_p$. This is due to the fact that the network is not large enough for the random phases to completely cancel, even when averaged over three sets of initial starting values.

We have also computed the dynamic structure factor $S(\mathbf{k},\omega)$. It is closely related to the coherent cross section defined in Eq. (31), and is obtained from it by setting the coherent scattering lengths $a_i^{\rm coh}$ equal to unity, i.e.,

$$S(\mathbf{k},\omega)=-\frac{1}{\pi}\mathrm{Im}\left[\sum_{i,j,\alpha,\beta}\hat{k}_\alpha\hat{k}_\beta G_{\alpha\beta}(i,j,\omega)e^{i\mathbf{k}\cdot\mathbf{R}_{ij}}\right]. \quad (120)$$

$S(\mathbf{k},\omega)$ was computed for the same wave vectors as $\epsilon(\mathbf{k},\omega)$, i.e., $\mathbf{k}=2\pi(0,0,\kappa)/L$, with $\kappa=1,2,3,5$. The results are shown in Fig. 9. We note a well-defined acoustic peak at $\omega=0.10\omega_p$ with a FWHH of $0.09\omega_p$ (after deconvolution with the resolution function) for the longest wavelength accessible in our system. Assuming a linear dispersion in this region, we obtain a longitudinal sound velocity $v_s=7.7$ km/sec, approximately 25% larger than the experimentally measured value in v-SiO_2.[37] This is due to the deficiencies in our force constant model, where we chose the parameters to give a reasonable description of the higher-frequency modes. The acoustic response broadens considerably at shorter wavelengths. For the shortest wavelength studied ($\kappa=5$) the spectrum is characterized by a broad band in the region $\omega\lesssim 1.1\omega_p$ and a peak at $\omega=1.16\omega_p$. One expects $S(\mathbf{k},\omega)$ to become increasingly similar to the density of states as the wavelength is decreased, because the phase factors $\exp(i\mathbf{k}\cdot\mathbf{R}_{ij})$

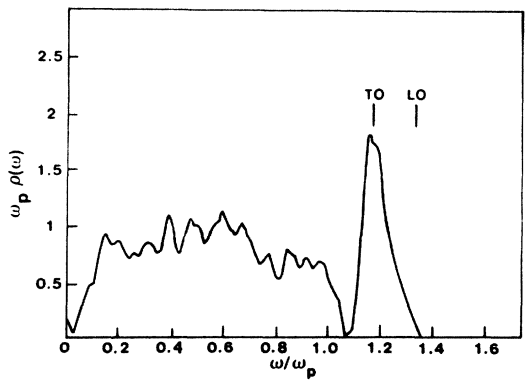

FIG. 8. Density of states $\rho(\omega)$ for the random network with LO and TO marking the peak positions of the dielectric response from Fig. 5.

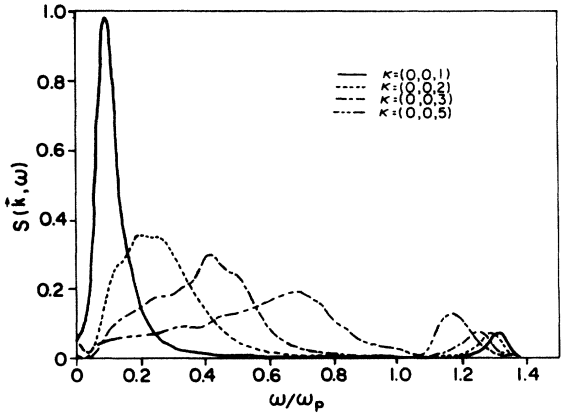

FIG. 9. Dynamic structure factor $S(\mathbf{k},\omega)$ for the random network for wave vectors $\mathbf{k}=2\pi(0,0,\kappa)/L$.

in Eq. (119) will effectively become randomized. Finally, we note that in the long-wavelength limit $S(\mathbf{k},\omega)$ shows a (small) peak at the longitudinal-optic frequency. As in crystalline materials, a coupling to transverse vibrations is only observed when the wavelength is sufficiently short (in crystalline materials one has to choose $\mathbf{k}$ outside the first Brillouin zone).

IX. CONCLUSIONS

We have shown how to include Coulomb forces in calculations of the vibrational responses in disordered solids like glasses and mixed crystals. The formalism is quite general and can be applied to any disordered solid. A number of interesting general relations and sum rules have been derived. These should be of considerable value in analyzing experimental data. The weight under the imaginary part of the dielectric function was shown in Eq. (62) to be

$$\omega_p^2=\frac{4\pi}{\Omega}\sum_i \frac{q_i^2}{m_i} ,$$

which we refer to as the *bare* plasma frequency. The second-moment relation $\langle\omega^2\rangle_l-\langle\omega^2\rangle_t=\omega_p^2/\epsilon_\infty$ given in Eq. (66) can be used to verify that the data is being analyzed consistently as ϵ_∞ can be obtained either by Kramers-Kronig analysis or by independent measurement. The generalized LST relation,

$$\frac{\epsilon_0}{\epsilon_\infty}=\left\langle\frac{1}{\omega^2}\right\rangle_t\Big/\left\langle\frac{1}{\omega^2}\right\rangle_l ,$$

Eq. (73), also involves the static dielectric constant ϵ_0 and can be used as a consistency check. Care must be used with the low-frequency part of the average $\langle 1/\omega^2\rangle$. Finally, the independence of the "width" $\langle\omega^4\rangle-\langle\omega^2\rangle^2$ to whether the longitudinal or transverse response is involved, Eq. (68), provides another consistency check.

Early numerical attempts to study LO-TO effects in glasses did not treat the long-range part of the Coulomb interactions correctly[5] and thus led to misleading results.[38] Attempts to develop analytic theories[6] have not been very successful to date. Hopefully, this work will encourage more efforts in this direction to increase our understanding and aid in the interpretation of experiments.

In this paper we have illustrated our general approach with numerical computations for a network glass. Preliminary accounts of this work has been published elsewhere.[38,39] In the future we hope to apply this technique to mixed semiconductor crystals and also to include polariton effects.

ACKNOWLEDGMENTS

We would like to thank R. J. Elliott, F. L. Galeener, S. D. Mahanti, and J. C. Phillips for many useful conversations on this problem. We would especially like to thank H. He for constructing the 1536-atom periodic network which is described in Sec. VII. The support of the U.S. Office of Naval Research (ONR) under Contract No. N00014-80-C-0610 is gratefully acknowledged. We also thank Colorado State University for the use of the Control Data Corporation Cyber 205 computer.

*Present address: Laboratorium voor Fysische Chemie, Universiteit van Amsterdam, Nienwe Achtergracht 127, 1018 WS Amsterdam, Netherlands.

[1]H. Bilz and W. Kress, in *Phonon Dispersion Relations in Insulators,* Vol. 10 of *Springer Series in Solid-State Sciences* (Springer-Verlag, Berlin, 1979), p. 105. The experimental data are from J. L. T. Waugh and G. Dolling, Phys. Rev. **32**, 2410 (1963).

[2]P. P. Ewald, Ann. Phys. (Leipzig) **64**, 253 (1921); see also E. W. Kellermann, Philos. Trans. R. Soc. London **238**, 513 (1940).

[3]See, for example, J. R. Hardy and A. M. Karo, *The Lattice Dynamics of Statics of Alkali Hailde Crystals* (Plenum, New York, 1979).

[4]F. L. Galeener and G. Lucovsky, Phys. Rev. Lett. **37**, 1477 (1976); F. L. Galeener, A. J. Leadbetter, and M. W. Stringfellow, Phys. Rev. B **27**, 1082 (1983).

[5]R. M. Pick and M. Yvinec, in *Proceedings of the International Conference on Lattice Dynamics, Paris, 1977,* edited by M. Balkanski (Flammarion, Paris, 1977).

[6]K. Sekimoto and T. Matsubara, Phys. Rev. B **26**, 3411 (1982); M. C. Payne and J. C. Inkson, J. Non-Cryst. Solids **68**, 351 (1983); A. Lehman, L. Schumann, and K. Hübner, Phys. Status Solidi B **117**, 689 (1983).

[7]M. Born and K. Huang, *Dynamical Theory of Crystal Lattices* (Oxford University Press, London, 1954), p. 248.

[8]A. A. Maradudin, E. W. Montroll, G. H. Weiss, and J. P. Ipatova, *Solid State Physics Supplement 3* (Academic, New York, 1971), Chap. 6.

[9]R. J. Elliott, J. A. Krumhansl, and P. L. Leath, Rev. Mod. Phys. **46**, 465 (1971); D. N. Zubarev, Usp. Fiz. Nauk. **71**, 71 (1960) [Sov. Phys.—Usp. 3, 320 (1960)].

[10]M. F. Thorpe, in *Vibrational Spectroscopy of Molecular Liquids and Solids,* NATO Advanced Study Institute Series B, edited by S. Bratos and R. M. Pick (Plenum, New York, 1980), p. 341.

[11]W. Marshall and S. W. Lovesey, *Theory of Thermal Neutron Scattering* (Oxford University Press, London, 1971).

[12]R. Barrio, R. J. Elliott, and M. F. Thorpe, J. Phys. C **16**, 3425 (1983).

[13]See, for example, N. D. Mermin and N. W. Ashcroft, *Solid State Physics* (Holt, Rinehart and Winston, New York, 1976).

[14]S. W. de Leeuw, J. W. Perram, and E. R. Smith, Proc. R. Soc. London, Ser. A **373**, 27 (1980).

[15]E. R. Smith, Proc. R. Soc. London, Ser. A **375**, 475 (1980).

[16]B. U. Felderhof, Physica **101A**, 275 (1980).

[17]E. T. Whittaker and G. W. Watson, *A Course of Modern Analysis* (Cambridge University Press, London, 1963), Chap. 21.

[18]G. A. Stratton, *Electromagnetic Theory* (McGraw-Hill, New York, 1941), p. 214.

[19]A. Rahman and P. Vashishta, in *The Physics of Superionic Conductors and Electrode Materials,* NATO Advanced Study Institute Series B92, edited by J. W. Perram (Plenum, New York, 1983), p. 93.

[20]A. L. Fetter and J. D. Walecka, *Quantum Theory of Many-Particle Systems* (McGraw-Hill, New York, 1971), p. 322.

[21]R. M. Lyddane, R. G. Sachs, and E. Teller, Phys. Rev. **59**, 673 (1941).

[22]A. S. Barker, Phys. Rev. **136**, 1290 (1964).
[23]M. F. Thorpe and R. Alben, J. Phys. C **9**, 2555 (1976).
[24]D. Beeman and R. Alben, Adv. Phys. **26**, 339 (1977).
[25]F. Wooten and D. Weaire, J. Non-Cryst. Solids **64**, 325 (1984); F. Wooten, K. Winer, and D. Weaire, Phys. Rev. Lett. **54**, 1392 (1985).
[26]S. W. de Leeuw, H. He, and M. F. Thorpe, Solid State Commun. **56**, 343 (1985).
[27]H. He, Ph.D. thesis, Michigan State University, 1985 (unpublished).
[28]F. H. Stillinger and T. A. Weber, Phys. Rev. B **31**, 5262 (1985).
[29]P. N. Keating, Phys. Rev. **145**, 637 (1966).
[30]J. F. Scott and S. P. S. Porto, Phys. Rev. **161**, 903 (1967).
[31]M. E. Striefler and G. E. Barsch, Phys. Rev. B **12**, 4553 (1975); T. H. K. Barron, C. C. Huang, and A. Pastenak, J. Phys. C **9**, 3925 (1976); J. Etchepare and M. Meriam, J. Chem. Phys. **68**, 5336 (1978).
[32]R. Fletcher, *Practical Methods of Optimization* (Wiley, New York, 1980).
[33]J. A. Erwin, A. C. Wright, J. Wong, and R. N. Sinclair, J. Non-Cryst. Solids **51**, 57 (1982).
[34]L. Verlet, Phys. Rev. **159**, 98 (1967).
[35]S. W. de Leeuw and J. W. Perram, Physica **107A**, 179 (1981).
[36]D. L. Price and J. Carpenter, Phys. Rev. Lett. **54**, 441 (1985).
[37]O. L. Anderson, J. Phys. Chem. Solids **12**, 41 (1959).
[38]S. W. de Leeuw and M. F. Thorpe, Phys. Rev. Lett. **55**, 2879 (1985).
[39]S. W. de Leeuw and M. F. Thorpe, J. Non-Cryst. Solids **75**, 393 (1985).